FORM TI-12
12/97

WAPD-T-3124

CONF-980708--

FATIGUE CRACK GROWTH TESTING OF SUB-CLAD DEFECTS

D. P. Jones and T. R. Leax

DE-AC11-93PN38195

NOTICE

BETTIS ATOMIC POWER LABORATORY WEST MIFFLIN, PENNSYLVANIA 15122-0079

Operated for the U.S. Department of Energy
by WESTINGHOUSE ELECTRIC COMPANY,
a division of CBS Corporation

(This Page Intentionally Blank)

DISCLAIMER

Fatigue Crack Growth Testing of Sub-Clad Defects

D. P. Jones & T. R. Leax
Westinghouse Electric Company
A Division of CBS
West Mifflin, PA 15122-0079

ABSTRACT

Fatigue crack growth tests were performed on four-point bend specimens with crack-like defects intentionally placed in A302B low-alloy pressure vessel steel clad with 308/309L weld deposited stainless steel. The defects were placed in the base metal under the cladding by machining a cavity from the side opposite the cladding, electric-discharge machining a very sharp flaw, fatigue pre-cracking the flaw, and then filling up the cavity by a weld repair process. The specimens were stress relieved before fatigue testing. The specimens were fatigue cycled at positive load ratios until the defects broke through to the surface. The specimens were then fractured at liquid nitrogen temperatures to reveal the fracture surfaces. Seven different sub-clad flaw specimens were tested in room temperature air and each test provides a record of cycles to defect break-through. Changes in defect size and shape as a function of applied load cycles were obtained by beach-marking the crack at various stages of the load history. The results provide a set of embedded defect data which can be used for qualifying fatigue crack growth analysis procedures such as those in Section XI of the ASME Boiler and Pressure Vessel Code. A comparison between calculated and measured values shows that the ASME B&PV Section XI fatigue crack growth procedures conservatively predict cycles to defect break-through for small sub-clad defects.

NOMENCLATURE

EDM Electric Discharge Machining
BWR Boiling water reactors
PWR Pressurized water reactors
FEA Finite Element Analysis
FCG Fatigue Crack Growth
Code ASME Boiler and Pressure Vessel Code
E Young's modulus
P Applied load
K Fracture mechanics stress intensity factor
K_{max} and K_{min} Maximum and Minimum Stress Intensity factors during a stress cycle
R-Ratio K_{min}/K_{max}
N Cycles
a Length of the minor axis of the defect
b One-half the length of the major axis of the defect
h Distance from the surface to the center of the defect
e Distance from the surface to the back of the EDM notch

t_c Thickness of the cladding
t Total thickness of the bend bar including cladding
l Length between the supports of the 4-point bend bar
da/dN Fatigue crack growth rate
σ Stress
C_1, n Constants in the fatigue crack growth rate correlation
ν Poisson's ratio
z Distance from mid-thickness including the cladding
l_0 Initial ligament between the precrack and the cladding

INTRODUCTION

Pressure vessels used to contain fluids that can aggressively attack carbon steels are often fabricated by weld overlaying the inside surface of the vessel with a corrosion resistant material such as an austenitic stainless steel. The cladding can be applied either to protect the contained fluid from contamination by the ferritic carbon steel or to protect the carbon steel from environmentally assisted cracking.

Although a defect free monolithic vessel of corrosion resistant material is preferred in most cases from a safety standpoint, economics or fabrication limitations often dictate that it is more practical to weld overlay corrosion resistant cladding material onto a less expensive carbon steel vessel. This is the standard fabrication process used for thick commercial nuclear pressure vessel construction. Typically, such vessels are built of a low-alloy pressure vessel steel with a thin (about 6-10 mm thick) weld deposited stainless steel cladding on the inside surface.

Unfortunately, weld deposition processes may produce defects in the base metal just under the first pass of the weld overlay. These defects are typically referred to as reheat cracks. The impact of small defects from reheat cracking in stainless-steel clad vessels has been recognized as a technical concern for maintenance of BWR and PWR vessels.

The purpose of this paper is to provide fatigue crack growth data that can be used to qualify analytic approaches for predicting life to cladding break-through from sub-clad cracks. As an example, measured cycles to break-through were compared to calculated values using the fatigue crack growth [FCG] procedures of Section XI of the ASME Boiler and Pressure Vessel Code. This analysis demonstrated that those procedures conservatively predict cycles to defect break-through for these tests.

LITERATURE

Many papers have been written on this subject. For example, the papers by Wimunc (1966), Vinckier and A.W. Pense (1974), and Canonico (1977) discuss the experience in the United States; the paper by Kondo, Nakajima and Nagasake (1971) discusses the Japanese experience on clad cracking in BWRs; the report by Druce and Hudson (1982) discusses the work done in the United Kingdom; and the paper by Bernard, *et. al.* (1989) is typical of the work done in France.

These papers conclude that the growth of sub-clad defects is slow and that the presence of such defects is tolerable as long as the defects do not break-through to the surface exposing the crack to the environment.

This paper provides data that can be used to qualify the fatigue crack growth technology used for predicting when sub-clad defects will break-through to the surface. The major short-coming of previous work has been uncertainties associated with determining when a sub-clad defect begins to grow as a fatigue crack since most experimental work has been done on actual weld induced defects or on manufactured defects that were weld overlaid. No matter how carefully these defects

are produced, it is always difficult to know when to begin to count crack growth cycles versus crack initiation cycles. Clearly assigning too much time to crack initiation can be unconservative if actual in-situ defects are more crack-like than the flaws produced in the laboratory.

The current paper provides additional data for use in qualifying computational methods for predicting sub-clad crack break-through obtained using test specimens and test procedures that reduce the difficulty in differentiating initiation cycles from growth cycles. This was accomplished by placing defects under sound cladding in such a way that the initially fatigue pre-cracked defect geometry was as undisturbed as possible prior to the start of the fatigue crack growth part of the test. In addition, beach-marks visible on the crack surface allowed a clear indication of crack growth versus crack initiation relative to measured cycles to break-through.

TEST METHOD

The purpose of this test program was to study the growth of cracks from the base-metal into and through the cladding. Accordingly, four-point bend bars were used for the testing because the bending stress increases from the base material to a maximum in the cladding thus driving sub-clad defects into the cladding. Also, the defects were placed in the base metal just under the cladding in such a way that the cladding and the defect front near the cladding were well defined. Figure 1 shows the specimen and defect geometry.

To achieve a well-defined sub-clad defect and undisturbed clad-base-metal interface, defects were placed in the base metal just beneath the cladding surface by machining out a cavity in the base metal to allow a sharp notch to be EDMed in the base metal without disturbing the clad-base metal interface. The notch was then fatigue pre-cracked and the cavity weld repaired. The specimens were heat treated after the weld repair for two hours at 1150°F to remove weld residual stresses. The process used to fabricate the specimen is shown schematically in Figure 2.

A beach-marking procedure was used to mark the fracture surface so that post-test crack length measurements could be made. The beach-marking process involved maintaining the maximum load and increasing the minimum load and frequency to place a mark on the fracture surface of about 0.025 mm. The tests were all conducted at room temperature using positive load ratios.

Figure 1a. Specimen Geometry.

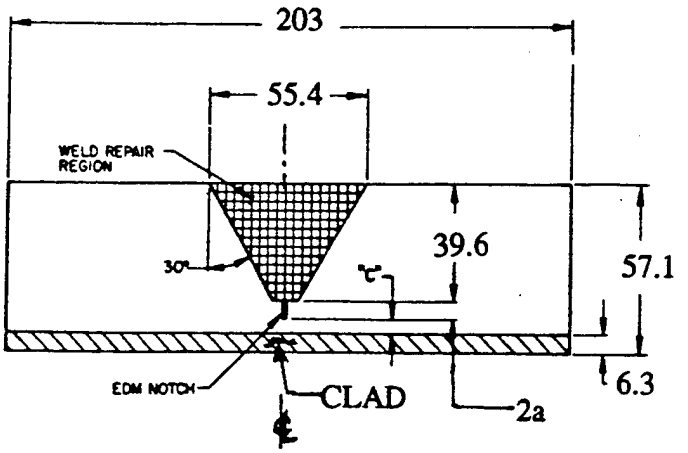

Figure 1b. Defect Geometry.

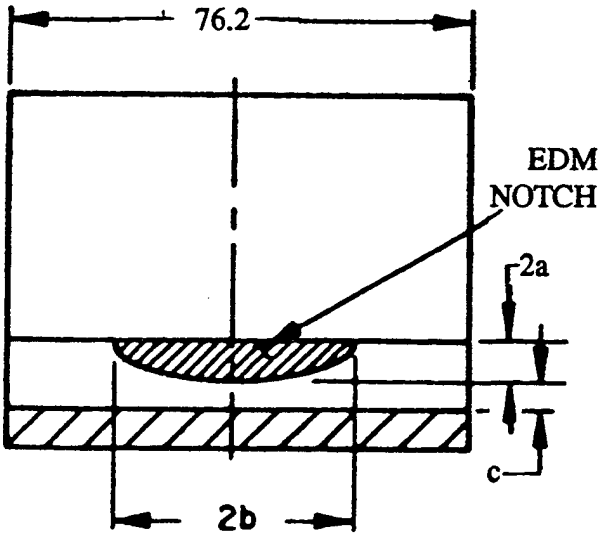

Two types of sub-cladding cracks were tested: cracks whose crack-fronts were initially about one crack depth (a) beneath the cladding thickness and cracks whose crack fronts were initially just at the clad-base metal interface. Table 1 provides measurements of the crack size and proximity to the clad-base-metal interface for the seven sub-cladding defect specimens. These dimensions were obtained from post-test measurements after the specimens were broken apart to reveal the fracture surface.

Table 1: Specimen Dimensions and Identification Numbers.

Specimen ID	Description		Defect Geometry,[mm]		
		l_0, mm	a, mm	b, mm	h, mm
LUC-1	Large Sub-Clad Defect	2.2	3.0	18.8	11.6
LUC-2	Large Sub-Clad Defect	2.4	2.9	18.8	12.6
LUC-3	Large Sub-Clad Defect	0	2.8	18.9	10.7
LUC-4	Large Sub-Clad Defect	0.6	3.0	18.6	10.7
LUC-5	Large Sub-Clad Defect	0	2.8	18.6	9.1
SUC-1	Small Sub-Clad Defect	1.3	1.3	4.5	9.1
SUC-2	Small Sub-Clad Defect	0	1.5	4.6	77.8

Figure 2. Specimen Fabrication.

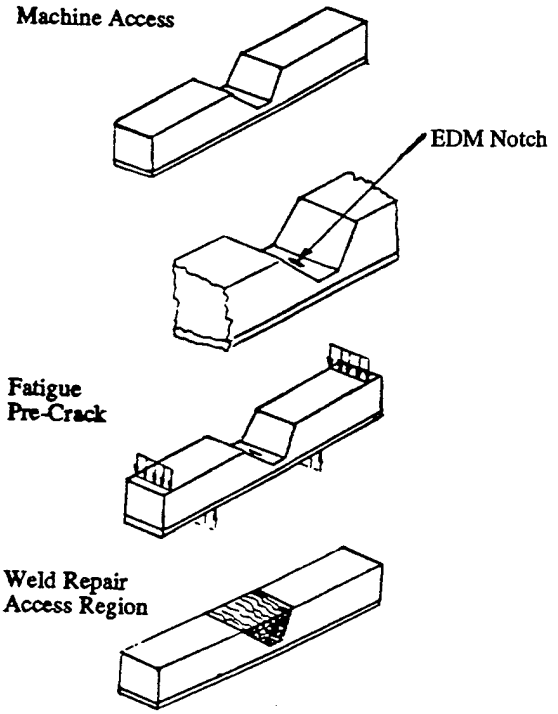

After weld repairing, the specimens were heat treated for two hours at 1150°F. Residual stresses were measured in one of the specimens using the layer removal technique and the results are shown in Figure 3. The residual stress distribution and magnitude are typical of residual stresses expected in post-stress relieved weld deposited cladding on wrought low-alloy steel. The stress relief appears to have successfully removed nearly all residual stresses due to the weld repair process.

MATERIALS

The base metal for the specimens was A302B low-allow pressure vessel steel. The steel had a room temperature yield strength of 411 MPa and an ultimate strength of 567 MPa with 25.3% elongation and 68.1% reduction in area. The cladding material is 308/309L stainless steel. It was applied in multi-layers using a submerged arc

Figure 3. Measured Residual Stresses.

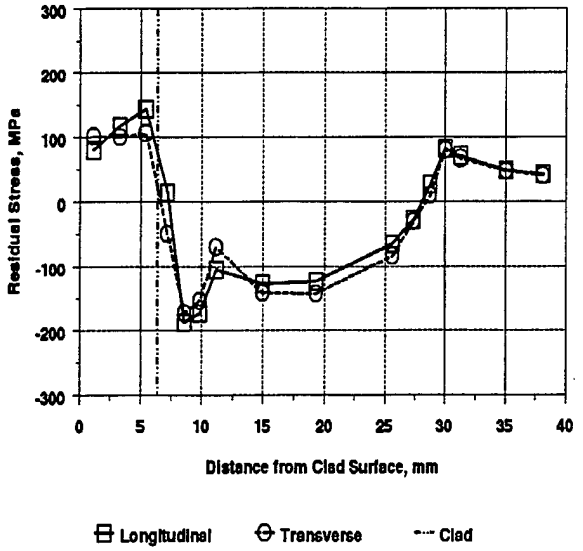

process similar to commercial pressure vessel practice. Three tests were performed to measure mechanical properties of the cladding material and the results of these tests are provided in Table 2.

Table 2: Tensile Properties of 308/309L Cladding Material

Specimen	Yield Strength, MPa	Tensile Strength, MPa
C1	303	544
C2	308	550
C3	310	549
Avg	307	548

FATIGUE TEST PROCEDURES

A four-point loading arrangement as shown in Figure 4 was used for these tests. This arrangement places the cracked test section in nearly pure bending. The tests were all run so that the bending stresses on the outer fiber of the beam (@ z=t/2) were equal to or less than the yield strength of the base material.

The fatigue tests were conducted by Materials Engineering Associates [MEA] using the four-point bend fixture shown in Figure 5. Fatigue cycling was performed in a 200 kip [890 kN] MTS closed loop servo-hydraulic machine with advanced electronic control. The advanced electronic control allowed the applied cyclic load to be controlled to within +/- 0.1 kips [0.4 kN] at both maximum and minimum load points. The

Figure 4. Four-Point Bend Test.

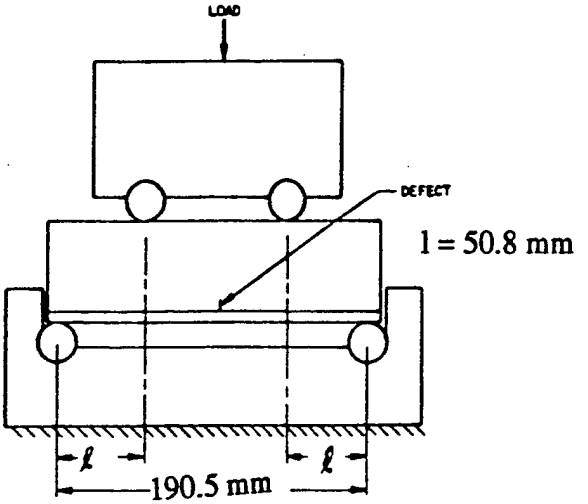

load signal was a sine wave at a frequency of 12 Hz for main fatigue crack propagation cycling. The tests were conducted at ambient temperature using a load ratio (P_{min}/P_{max}) of 0.1 for all but the beach marking cycles.

The tests were run until there was a visible crack on the outside of the cladding surface. Strain gauges were placed on the outside surface directly over the location of expected break-through and moment deflection (compliance) measurements were taken during the test. Once there was a visible surface crack, the fatigue tests were terminated and the specimens were broken apart after soaking in liquid nitrogen. The specimens all showed very flat cleavage fractures.

As mentioned, beach-marking was used to

periodically mark the crack front during the test to provide crack size data at various cycle numbers. The beach-marking procedure consisted of maintaining the maximum load and adjusting the minimum load so that the load ratio was 0.5. The cyclic frequency was increased to 20 Hz during beach-marking. By trial and error, the number of beach mark cycles was adjusted to produce a beach-mark zone of about 0.025 mm.

Figure 5. Test Fixture.

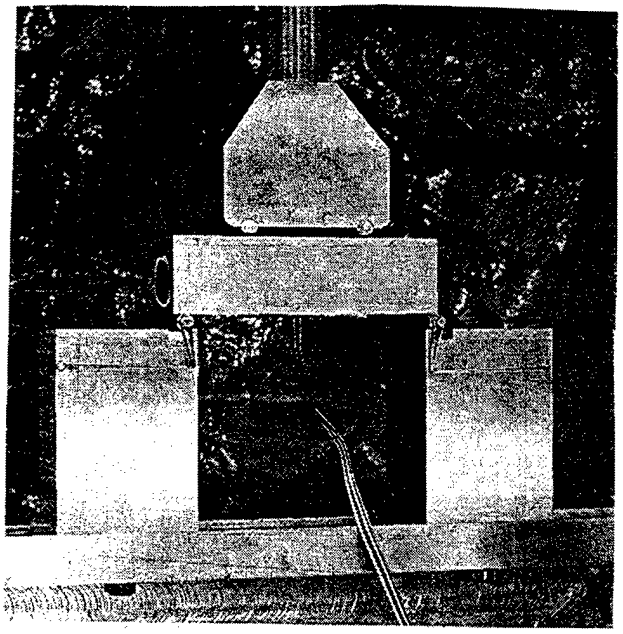

After the fatigue crack growth tests, the specimens were broken apart to reveal the fracture surface. Crack length versus cycles records were then established by working backwards from the final size by correlating beach-marks with main load-cycle blocks. Since crack extension was basically blind until after the test was complete and the specimens broken apart, the method was first demonstrated on surface flaw specimens. Also, each sub-clad specimen was broken apart before proceeding to the next specimen to assure that sufficiently visible beach-marks were produced.

RESULTS

Figure 6 shows the crack measurement locations of the sub-clad embedded defect geometry used to determine the crack dimensions for each specimen. The large under-clad cracks were tested first. Results for specimens LUC-1, LUC-2, LUC-3, LUC-4 and LUC-5 are listed in Tables 3-7. The results for the small sub-clad defects SUC-1 and SUC-2 are listed in Tables 8 and 9. The fracture surfaces of the specimens are shown in Figures 7 through 13.

The specimens were very stiff and so crack size had very little influence on the load-deflection curve. There was virtually no difference in compliance for the LUC specimens and the SUC specimens. There was no early warning of surface cladding break-through either by changes in compliance, changes in surface strain gauge readings, or by surface appearance. The surface appeared undisturbed until the defect broke through.

Figure 6. Sub-Clad Crack Geometry.

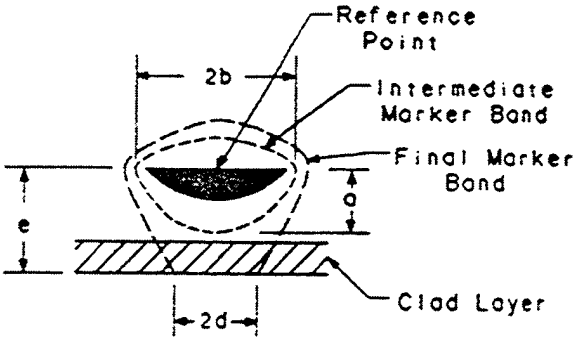

The first specimen tested was LUC-1. The pre-test load range chosen produced a break-through before any beach-marking cycles. The test was continued after break-through and the crack was grown in fatigue as a surface defect until the flaw reached a depth of nearly 50% through the specimen.The fracture surface is shown in Figure 7 while Table 3 provides crack measurements and load cycles.

For tests LUC-2 through LUC-5, SUC-1 and SUC-2, either smaller load ranges or fewer cycles between main load blocks were used and beach marks were present to show the progression of the initial sub-clad defect to break-through. Fracture surfaces for these tests are shown in Figures 8-13. The results indicate that crack growth accelerated in the cladding material as the crack approached the surface as evidenced by the wider beach-marks in the cladding compared to those in the base metal. This is the apparent result of the higher bending stresses in the cladding, an increased ΔK due to the larger flaw size, the positive residual stress in the cladding elevating the R-ratio and thus accelerating the FCG rate, and the higher FCG rate of the stainless steel cladding material compared to the base metal.

The fracture surfaces also show no apparent retardation of the FCG rate as the crack front advances through the base metal in the region just under the clad-base metal interface as might be expected as a result of the compressive residual stress in the base metal near the clad-base metal interface.

Both specimens SUC-1 (Figure 12) and SUC-2 (Figure 13) have large spacing between beach-marks as the crack approached the neutral surface of the beam (i.e., in the direction away from the cladding). This suggests that local residual stresses may be present in the weld repair region even though the residual stress measurements showed that the residual stresses were small in the weld-repair region. Even if tensile residual stresses are present in the weld repair region, they only appear to have affected crack growth in the direction away from the cladding and so did not compromise the test purpose which was to observe growth of the defects from base-metal into and through the cladding material. Both the large and small sub-clad defects grew as expected

through the clad-base metal interface suggesting that the residual stress distribution had little influence on the da/dN rate.

DISCUSSION

The results can be used to qualify FCG computational procedures by comparison of the crack size versus cycles data and cycles to break-through with calculated results obtained by integrating da/dN correlations with ΔK. Bernard, *et. al.* (1989) provide an example of this using the data generated in that work.

The results of such a comparison depend significantly on the ΔK solution for the embedded defect and on the da/dN correlation. Most stainless steel power-law correlations result in da/dN being proportional to ΔK^n where n is between 3 and 4. For this reason, the range of the stress intensity factor (ΔK) is particularly critical. As the defect intersects the cladding-base metal interface, multi-material considerations come into play and as the defect approaches the outer surface, near surface yielding and other uncertainties become significant. The calculated cycles-to-break-through therefore depends on both the FCG rate curve and the ΔK solution. If the ΔK solution is overly conservative, then agreement can be achieved by using a less conservative da/dN curve and vice-versa. The ΔK solution and the da/dN curve have to be taken together, at least until all uncertainty is removed from the technology. For embedded defects, both the ΔK solution and the appropriate da/dN curve for the sub-clad environment are under question.

An example of such calculations is provided here. The bending stress range in the test section of the four-point bend bar is:

$$\Delta\sigma_B = \Delta Pl/Bt^2 \qquad \text{Eq. (1)}$$

A stress intensity factor solution similar to the solution included in Article A-3000 for an

embedded elliptical defect was used so that:

$$\Delta K = \Delta\sigma_B M_B[\pi a/(1. + 1.464(a/b)^{1.65})]^{0.5} \quad \text{Eq. (2)}$$

In this equation, the crack length a is one-half the length of the minor axis or a/2. The magnification factor M_B is a function of crack geometry and solutions based on various approximations are widely available (see Section XI of the ASME Code). R-ratio effects are accounted for by adding the residual stress shown in Figure 3 to both the maximum and minimum stress and then calculating K_{min}/K_{max} for the load cycle. This information and the best estimate FCG rates for stainless steel in Article C-3000 of the Code allows the calculation of cycles-to-break-through for each test. Results obtained by defining break-through as the point where the ligament between the defect and the free-surface is 5% of the length of the minor axis are compared to the measured values in Figure 14. The results of the calculations are very conservative for small cracks (specimens SUC-1 and SUC-2) and reasonable for large cracks.

CONCLUSIONS

Qualitative observations made from these tests are:

(1) There were no early warnings of incipient crack break-through either by compliance changes, strain gauge readings, or surface indications.

(2) Fatigue crack growth rate accelerates through the cladding material as the crack approaches the free surface.

(3) The compressive residual stresses in the base metal near the clad-base metal interface do not appear to significantly retard the da/dN rates.

(4) Comparison of the test data with analytic solutions of crack size allows qualification of an analytic procedure which includes both the da/dN correlation and the stress intensity solution. Such calculations were performed using the da/dN curve from Section XI and show that the Section XI procedure is conservative for small sub-clad defects.

ACKNOWLEDGMENTS

This work was performed under a U.S. Department of Energy contract with the Bettis Atomic Power Laboratory, a unit of the Westinghouse Electric Company. The experimental work was performed under subcontract to Bettis by Materials Engineering Associates [MEA]. Mr. Donald E. McCabe was the principal investigator and his efforts are greatly appreciated.

REFERENCES

E.A. Wimunc, 1966, "How Serious Are Vessel Cladding Failures?," Power Reactor Technology, Vol. 9, pgs. 101-109.

Kondo, T., H. Nakajima, R. Nagasaki, 1971, "Metallographic Investigation on the Cladding Failure in the Pressure Vessel of a BWR," Nuclear Engineering and Design, Vol. 16, North-Holland Publishing Co., pgs. 205-222.

D.A. Canonico, 1977, "Significance of Reheat Cracks to the Integrity of Pressure Vessels for Light-Water Reactors," ORNL/NUREG 15, 1977.

Vinckier, A.G. and A.W. Pense, 1974, "A Review of Underclad Cracking in Pressure Vessel Components," WRC Bulletin 197, August.

Bernard, J.L., J. Vagner, A. Pellissier-Tanon, F. Faure, 1992,"Effect of Residual Stresses and Complex Loadings on the Fatigue Behav-

ior of Underclad Cracks," Nuclear Engineering and Design, Vol 133, pgs 3-15.

S. G. Druce and J. A. Hudson, 1982, "Defects Arising from Welding and Cladding PWR Pressure Vessel Steels - A Review," AERE - R 10418, Metallurgy Division, AERE Harwell, February.

Figure 7. Fracture Surface for Specimen LUC-1.

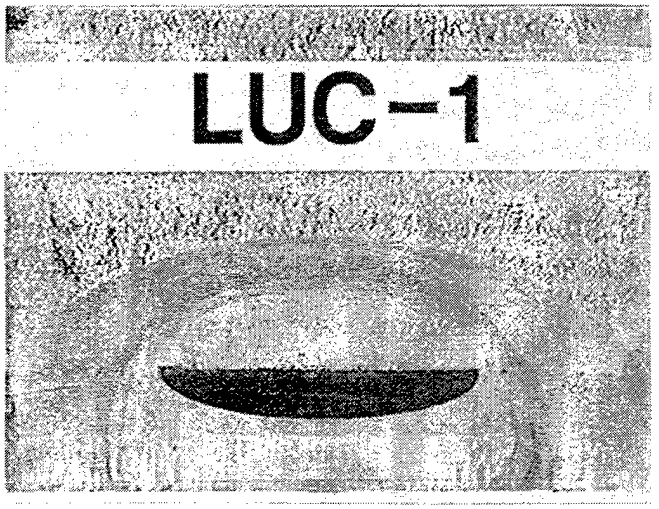

Figure 8. Fracture Surface for Specimen LUC-2.

Figure 9. Fracture Surface for Specimen LUC-3.

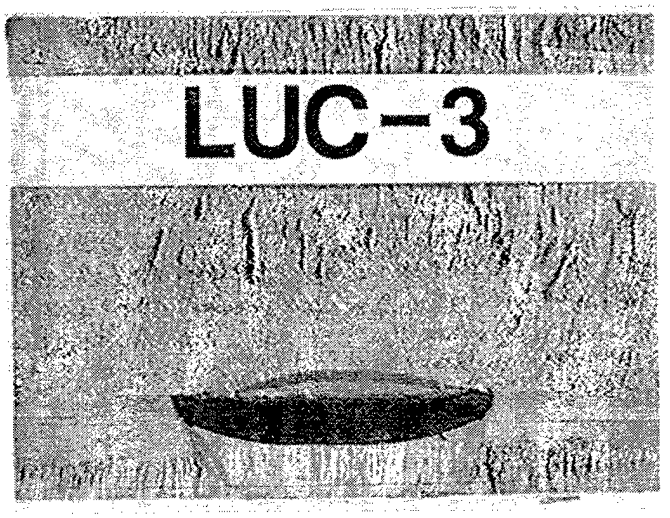

Figure 10. Fracture Surface for Specimen LUC-4.

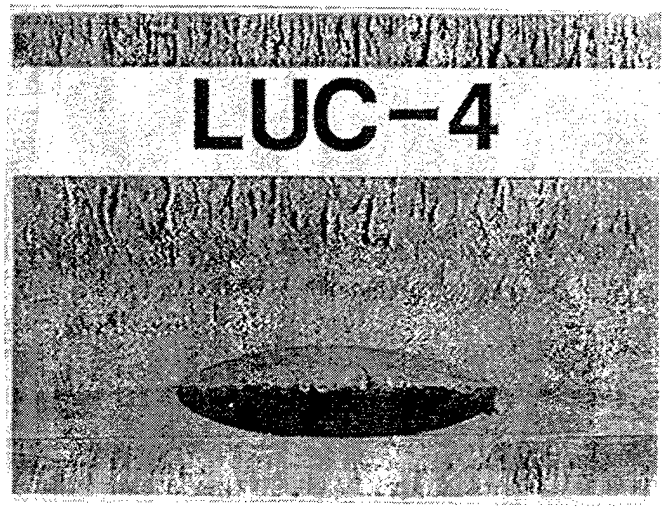

Figure 11. Fracture Surface for Specimen LUC-5.

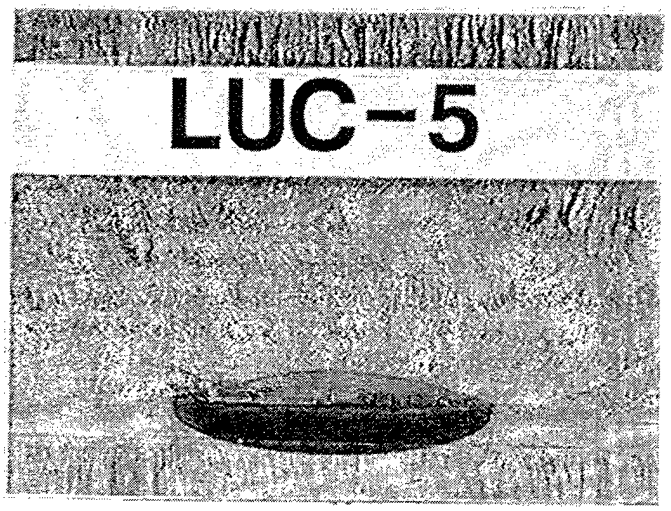

Figure 12. Fracture Surface for Specimen SUC-1.

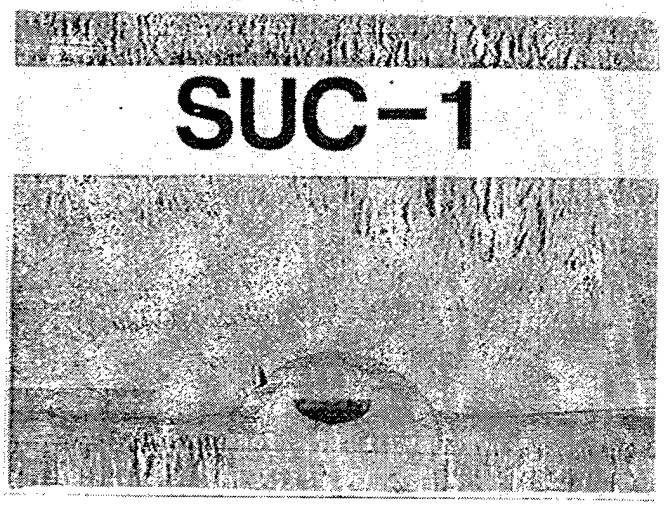

Figure 13. Fracture Surface for Specimen SUC-2.

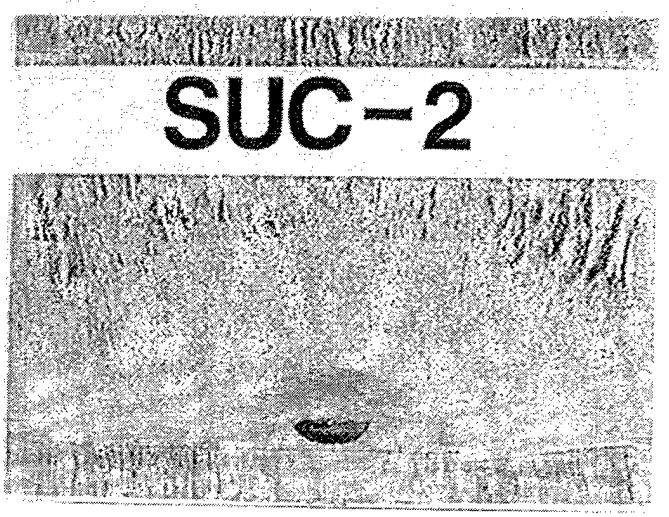

Figure 14. Comparison of Calculated and Measured Cycles to Break-Through.

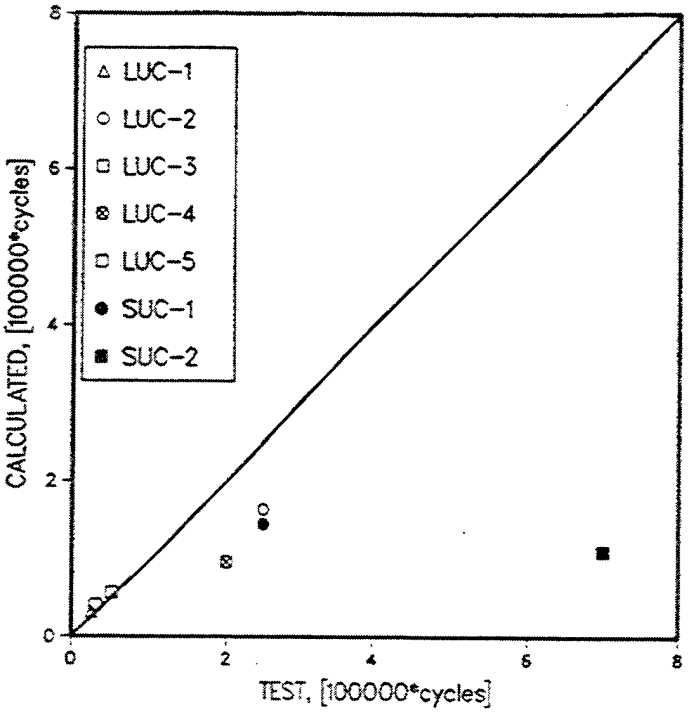

Table 3: Results for LUC-1

ΔP kN	R-ratio P_{min}/P_{max}	Cycles x1000	a mm	b mm	d mm	Comment
Initial			6.10	19.0		e = 14.8 mm
625	0.1	25		19.9	4.50	Break-thru
260	0.5	25		21.5	20.1	
312	0.1	25		22.8	23.7	
312	0.1	25				
173	0.5	100		25.1	25.3	
312	0.1	50				
173	0.5	25		31.8	34.4	

Table 4: Results for LUC-2.

ΔP kN	R-ratio P_{min}/P_{max}	Cycles x1000	a mm	b mm	d mm	Comment
Initial			5.94	18.9		e = 14.8 mm
374	0.1	50				
208	0.5	50	6.68	18.9		
374	0.1	50				
208	0.5	50	7.67	18.9		
374	0.1	50				
208	0.5	50	9.45	18.9		
374	0.1	50				
208	0.5	50	10.94	18.9		
374	0.1	50				
208	0.5	50	14.0	18.9		
374	0.1	50				Break-thru
208	0.5	50		18.9	15.5	

Table 5: Results for LUC-3.

ΔP kN	R-ratio P_{min}/P_{max}	Cycles x1000	a mm	b mm	d mm	Comment
Initial			5.71	19.0		e = 12.0 mm
400	0.1	30				
222	0.5	50		19.0	9.63	Break-thru
267	0.1	50				
148	0.5	50		19.0	11.9	

Table 6: Results for LUC-4.

ΔP kN	R-ratio P_{min}/P_{max}	Cycles x1000	a mm	b mm	d mm	Comment
Initial			6.09	18.8		e = 13.0 mm
340	0.1	50				
189	0.5	50	7.85	18.8		
340	0.1	50				
189	0.5	50	8.89	18.8		
340	0.1	50				
189	0.5	50	12.2	18.8		
340	0.1	50				
189	0.5	50		18.8	12.5	Break-thru
340	0.1	50				
189	0.5	50		18.8	16.2	

Table 7: Results for LUC-5

ΔP kN	R-ratio P_{min}/P_{max}	Cycles x1000	a mm	b mm	d mm	Comment
Initial			5.74	18.8		e = 11.5 mm
336	0.1	25			4.50	
187	0.5	50	8.31	18.8	20.1	
336	0.1	25	9.88	18.8	23.7	
187	0.5	50		18.8	5.46	Break-thru
336	0.1	25				
187	0.5	50		18.8	12.42	

Table 8: Results for SUC-1.

ΔP kN	R-ratio P_{min}/P_{max}	Cycles x1000	a mm	b mm	d mm	Comment
Initial			2.57	4.57		e = 10.0 mm
400	0.1	100				
222	0.5	100	5.84	4.57		
600	0.1	100				
334	0.5	100	8.64	6.71		
600	0.1	50				
334	0.5	50		7.62	2.44	Break-thru
500	0.1	25				
278	0.5	50		10.2	7.77	
400	0.1	50				

(This Page Intentionally Blank)

Report Number (14) WAPD-T--3124
CONF-980708--

Publ. Date (11) 199804
Sponsor Code (18) DOE/NE, XF
UC Category (19) UC-500, DOE/ER

No 1332.15 in folder

DOE